Polyhedron 30 (2011) 971–975

Contents lists available at ScienceDirect

Polyhedron

journal homepage: www.elsevier.com/locate/poly

Preparation and characterization of NiO nanoparticles from thermal decomposition of the $[Ni(en)_3](NO_3)_2$ complex: A facile and low-temperature route

Saeid Farhadi *, Zeinab Roostaei-Zaniyani

Department of Chemistry, Lorestan University, Khoramabad 68135-465, Iran

ARTICLE INFO

Article history:
Received 7 December 2010
Accepted 27 December 2010
Available online 9 January 2011

Keywords:
NiO nanoparticles
Tris(ethylenediamine)Ni(II)
Metal oxides
Thermal decomposition
Ferromagnetic behavior

ABSTRACT

NiO nanoparticles with an average size of 15 nm were easily prepared via the thermal decomposition of the tris(ethylenediamine)Ni(II) nitrate complex $[Ni(en)_3](NO_3)_2$ as a new precursor at low temperature, and the nanoparticles were characterized by thermal analysis (TGA/DTA), X-ray diffraction (XRD), Fourier-transformed infrared spectroscopy (FT-IR), UV–Vis spectroscopy, BET specific surface area measurement, scanning electron microscopy (SEM), energy-dispersive X-ray spectroscopy (EDX), transmission electron microscopy (TEM) and magnetic measurements. The magnetic measurements confirm that the product shows a ferromagnetic behavior at room temperature, which may be ascribed to a size confinement effect. The NiO nanoparticles prepared by this method could be an appropriate photocatalytic material due to a strong absorption band at 325 nm. This method is simple, fast, safe, low-cost and also suitable for industrial production of high purity NiO nanoparticles for applied purposes.

1. Introduction

Nanomaterials exhibit optical, catalytic, electronic and magnetic properties that are significantly different from those of the corresponding bulk materials [1–3]. Among these materials, transition metal oxides have attracted much attention due to their outstanding electrical, magnetic and catalytic properties [4]. Nickel oxide (NiO) is one of the most important transition metal oxides due to its applications in diverse fields, including the fabrication of p–n heterojunctions [5], catalysis [6,7], electrochromic films [8,9], fuel cell electrodes [10], gas sensors [11,12], battery cathodes [13,14], magnetic materials [15,16], photovoltaic devices [17], electrochemical capacitors [18] and smart windows [19]. Most of these applications require particles with a small size and a narrow size distribution. Because of the volume effect, the quantum size effect and the surface effect, NiO nanoparticles are expected to possess many improved properties and even more attractive applications than those of bulk-sized NiO particles.

There are many methods for the preparation of NiO nanoparticles, such as the coprecipitation method [20–22], microemulsion method [23,24], ultrasonic radiation [25], hydrothermal synthesis [26,27], anodic arc plasma method [28], microwave irradiation [29], sol–gel method [30–32], low pressure spray pyrolysis [33,34] amongst others. However, to the best of our knowledge, most of the reported techniques for the synthesis of NiO nanoparticles are still limited to the laboratory scale due to some unresolved problems, such as special conditions, tedious procedures, complex apparatus, need for expensive agents or special equipment, low-yield and high-cost. From a practical viewpoint, it is vital to develop a way to manufacture high-quality nanoparticles at a high throughput with low cost.

The solid-state thermal decomposition of complexes is one of the simplest and lowest-cost techniques for preparing pure and nanosized transition metal oxides with relatively high specific surface area at low temperature [35]. Because of the high degree of homogenization of the precursor, much lower temperatures are sufficient for the reaction to occur. This method exhibits many advantages; no need for solvent, surfactant and complex apparatus, high yield, low energy consumption and simple reaction technology. In this context, various simple and mixed metal oxides nanoparticles have been prepared by solid-state thermal decomposition of their corresponding complexes [36–39].

In this work, which is a continuation of our studies on the preparation of nanosized transition metal oxides via the decomposition of complexes [40,41], we wish to report our results on the thermal decomposition of the tris(ethylenediamine)Ni(II) nitrate complex $[Ni(en)_3](NO_3)_2$, which leads to the formation of pure NiO nanoparticles at low temperature. The product was identified by X-ray diffraction (XRD), Fourier-transformed infrared spectroscopy (FT-IR), UV–Vis spectroscopy, BET specific surface area measurement, scanning electron microscopy (SEM), energy-dispersive X-ray spectroscopy (EDX), transmission electron microscopy (TEM), thermal analysis (TGA/DTA) and magnetic measurements.

---

* Corresponding author. Tel.: +98 6612202782; fax: +98 6616200088.
E-mail address: sfarhad2001@yahoo.com (S. Farhadi).

0277-5387/$ - see front matter © 2011 Elsevier Ltd. All rights reserved.
doi:10.1016/j.poly.2010.12.044

2. Experimental

2.1. Preparation of materials

Although the $[Ni(en)_3](NO_3)_2$ complex is not commercially available, the synthesis is trivial and requires no specialized apparatus. An aqueous solution of commercial $Ni(NO_3)_2 \cdot 6H_2O$ is treated with a slight stoichiometric excess of ethylenediamine (en) and the resultant deep-purple $[Ni(en)_3](NO_3)_2$ was precipitated by slow addition of alcohol. After standing for several hours in the cold, the crystals were filtered on a Buchner funnel, washed with alcohol, ether, and dried in the open air at 50 °C. The complex was characterized by FT-IR, elemental analyses (C, H, N) and thermal analysis. Anal. Calc. for $[Ni(en)_3](NO_3)_2$: C, 19.85; H, 6.67; N, 30.82. Found: C, 20.04; H, 6.72; N, 30.80%.

In order to prepare NiO nanoparticles, the $[Ni(en)_3](NO_3)_2$ complex was decomposed at various temperatures for 1 h in ambient air. The temperatures for the decomposition of the complex in the range of 200–400 °C were selected from the results of the TGA-DTA analysis. The decomposition products were collected for characterization.

2.2. Characterization techniques

The XRD patterns were recorded by a Rigaku D-max C III, X-ray diffractometer using Ni-filtered Cu Kα radiation (λ = 1.5406 Å) to determine the phases present in the decomposed samples. Infrared spectra were recorded on a Shimadzu system FT-IR 160 spectrophotometer using KBr pellets. The elemental analysis (C, H, N) of the starting complex was performed using a Carlo Erba 1106 instrument. The thermal decomposition behavior of the precursor complex was studied by a Netzsch STA 409 PC/PG thermal analyzer at a heating rate of 10 °C/min in air. The optical absorption spectrum was recorded on a Shimadzu 1650PC UV–Vis spectrophotometer with the wavelength range 300–700 nm at room temperature. The sample for UV–Vis studies was well dispersed in distilled water to form a homogeneous suspension by sonication for 25 min. The powder morphology was observed by a scanning electron microscope (SEM, Philips XL30) equipped with a link energy-dispersive X-ray (EDX) analyzer. The particle size was determined by a transmission electron microscope (TEM, Philips CM10,) at an accelerating voltage of 80 kV. The powders were ultrasonicated in ethanol and a drop of the suspension was dried on a carbon-coated microgrid for the TEM measurements. The magnetic properties of the NiO nanoparticles were measured with a vibrating sample magnetometer (VSM) (BHV-55, Riken, Japan) at room temperature. The specific surface area of the product was measured by the BET method using a N_2 adsorption–desorption isotherm carried out at −196 °C on a Surface Area Analyzer (Micromeritics ASAP 2010). Before each measurement, the sample was degassed at 200 °C for 2 h.

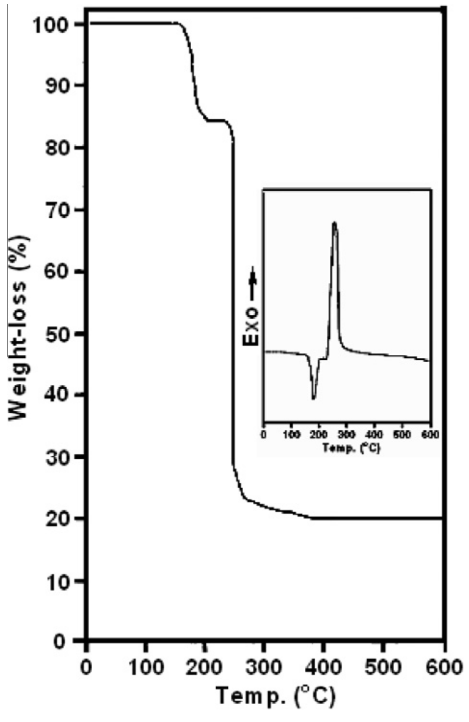

Fig. 1. Thermal analysis (TGA/DTA) of the $[Ni(en)_3](NO_3)_2$ complex.

3. Results and discussion

In order to obtain a better recognition of the thermal decomposition process of $[Ni(en)_3](NO_3)_2$, thermal analysis was done on this complex. Fig. 1 shows the TG and DTA curves recorded for $[Ni(en)_3](NO_3)_2$ at a constant heating rate of 10 °C min^{-1} in the temperature range 25–600 °C. The TG curve shows that the decomposition of the complex proceeds in two main stages. The first stage occurs at

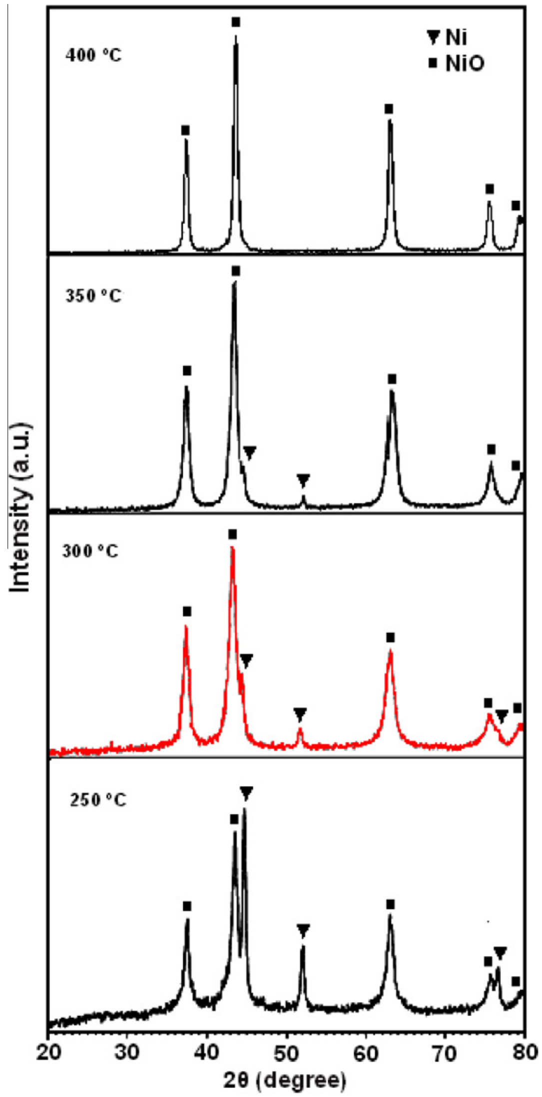

Fig. 2. XRD patterns of the $[Ni(en)_3](NO_3)_2$ complex decomposed at selected temperatures.

185 °C, showing a 16% weight-loss which is consistent with the theoretical value of 16.54% caused by the loss of one mole of ethylenediamine (en) per mole of complex. On further heating, the residue $[Ni(en)_2](NO_3)_2$ complex decomposed explosively at *ca.* 235 °C, followed by a gradual weight loss up to 380 °C. Above 400 °C, the weight remained constant, confirming the complete decomposition of the complex. The weight loss of all the steps was about 80%, which is consistent with the theoretical value (79.40%) calculated for the formation of NiO from the complex. The DTA curve for the $[Ni(en)_3](NO_3)_2$ complex, as shown in the inset of Fig. 1, gave two characteristic peaks, consistent with the TG data. The small endothermic peak at 185 °C can be explained by freeing one en molecule, resulting in the formation of the bis(ethylenediamine) complex, according to the following reaction:

$$[Ni(en)_3](NO_3)_2 \rightarrow [Ni(en)_2](NO_3)_2 + en \qquad \text{step I} \tag{1}$$

The big exothermic peak at about 235 °C is due to the explosive decomposition of $[Ni(en)_2](NO_3)_2$ complex via the redox process taking place between the reducing agent (en ligands) and the oxidizing agent (NO_3^-), leading to N_2, NO, N_2O, H_2O, and CO_2 gaseous products, according to the following reaction:

$$[Ni(en)_2](NO_3)_2 \rightarrow NiO + N_2 + N_2O + NO + CO_2 + H_2O \qquad \text{step II} \tag{2}$$

The XRD patterns of the complex and its decomposition products at various temperatures after 1 h are shown in Fig. 2. For the sample decomposed at 250 °C, peaks attributable to the metallic Ni phase (▼, JCPDS File No. 76-0147) and NiO (■, JCPDS Card No. 73-1523) are observed. At 300 °C, the characteristic peaks of cubic NiO appeared together with a decrease in the intensity of the Ni phase peaks. When the decomposition temperature increases to 350 °C, apparent diffractive peaks of nickel oxide appear with high intensity, and the diffractive peaks of metallic nickel become weakly evident. Finally, the XRD analysis for the sample decomposed at 400 °C, showed only the pattern corresponding to cubic NiO, with lattice constants *a* = 4.1771 Å (JCPDS, File No. 73-1523). This confirms that at this temperature the metallic nickel has changed completely to nickel oxide. No characteristic XRD peaks arising from other impurity phases are visible, indicating the preparation of pure NiO by the present method. It can be seen from Fig. 2 that the diffraction peaks are markedly broadened due to the small size effect of the particles. Furthermore, the width of the NiO peaks decreases with an increase in the decomposition temperature up to 400 °C, because of crystallite growth. The average size of the NiO particles was estimated to be about 15.5 nm by the Debye–Scherrer equation [42]: $D_{XRD} = 0.9\lambda/(\beta\cos\theta)$ where D_{XRD} is the average crystalline size, λ is the wavelength of Cu Kα, β is the full width at half maximum (FWHM) of the diffraction peak and θ is the Bragg's angle.

The FT-IR spectra of the complex samples decomposed at different temperatures are shown in Fig. 3. For the starting complex, the characteristic stretching bands of NH_2, CH_2, NO_3 are observed at about 3250–3500, 2850 and 1350 cm^{-1} [43]. As can be seen in Fig. 3, all of these bands disappear when the complex is heated up to 300 °C. At the same time, the bands attributable to carbonate groups are observed in the 1300–1500 cm^{-1} region for the samples decomposed up to 300 °C [43]. The intensity of these bands decreases with increasing temperature, so that all of them disappeared at 400 °C. From these data, it can be concluded that the carbonate groups are formed during the decomposition of the en ligands of complex, and their contents decrease with the increase of temperature. In the FT-IR of the product at 400 °C, the strong band at 435 cm^{-1} is assigned to the Ni–O stretching of the octahedral NiO_6 groups in the face center cubic structure [44]. It is noted that the peaks at 1600 and 3600 cm^{-1} in the FT-IR spectra of the samples decomposed at 300 °C should be assigned to H_2O absorbed by the samples or KBr.

The morphology of $[Ni(en)_3](NO_3)_2$ and its decomposition product at 400 °C were investigated by SEM. Fig. 4a and b show the SEM micrographs of the starting complex at two different scales. It is obvious that the starting complex powder was made of large crystals and grains with different shapes. The sizes of these grains are in the range of 0.5–3.5 µm. The SEM micrographs of the product powder in Fig. 4c and d clearly show that the shape and morphology of the NiO are quite different from that of the precursor com-

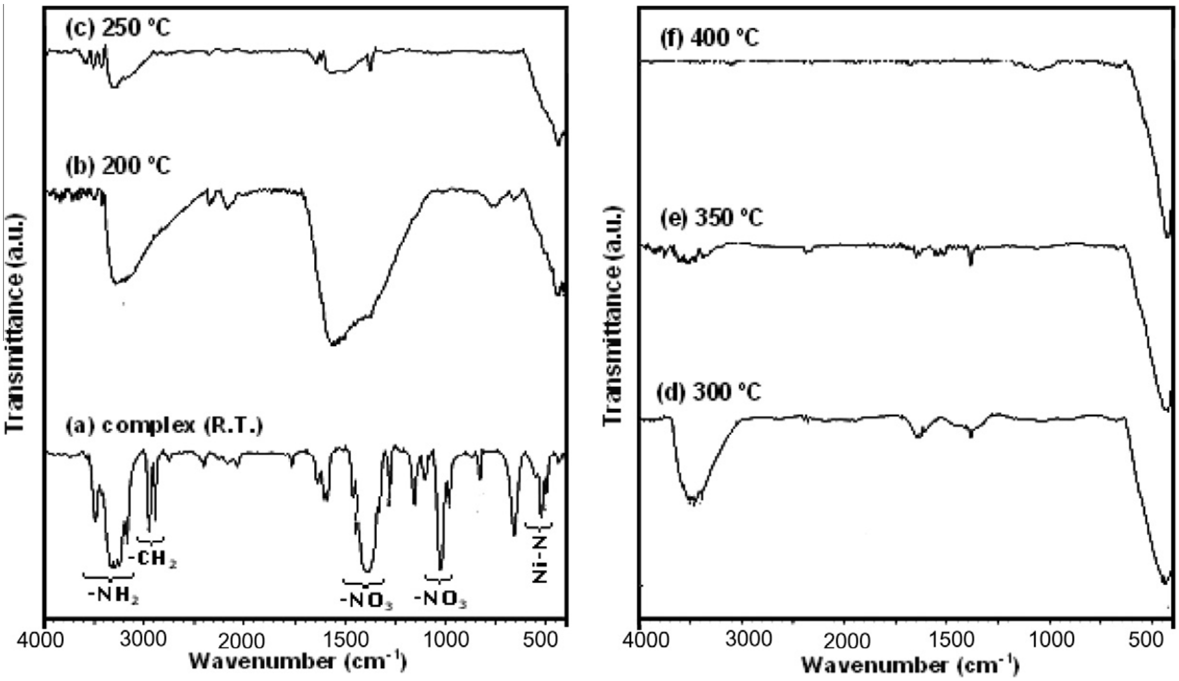

Fig. 3. FT-IR spectra of the $[Ni(en)_3](NO_3)_2$ complex decomposed at various temperatures.

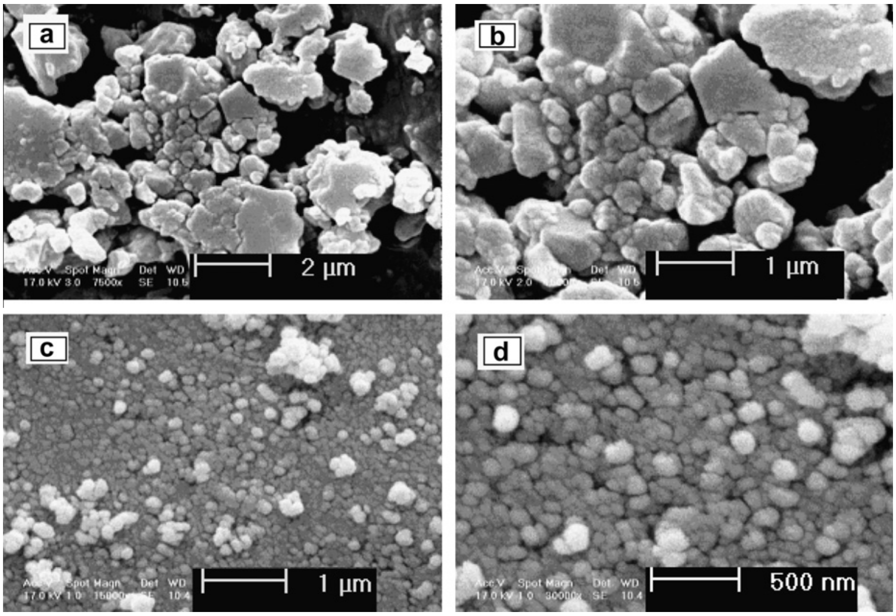

Fig. 4. SEM micrographs of the $[Ni(en)_3](NO_3)_2$ complex (a and b) and the NiO nanoparticles (c and d) at different scales.

plex. It can be seen that the product was formed from extremely fine spherical particles which were loosely aggregated. No characteristic morphology of the complex is observed, indicating complete decomposition into the extremely fine spherical particles.

Fig. 5 shows the TEM image of the NiO product. The TEM sample was prepared with the dispersion of powder in ethanol by ultrasonic vibration. It can be seen that the uniform NiO particles had spherical shapes with weak agglomeration. As shown in Fig. 5, the particle sizes possess a narrow distribution in a range from 10 to 20 nm, and the mean particle diameter is about 15 nm. Actually, the mean particle size determined by TEM is very close to the average particle size calculated by the Debye–Scherrer formula from the XRD pattern. Such consistence implies that the formed nanoparticles are single-phase.

The EDX analysis of the prepared NiO nanoparticles confirmed that the atomic percentages of Ni and O are 50.2% and 49.8%, respectively. Accordingly, the atomic ratio of Ni and O is about 1:0.98, which is consistent with the theoretical value of NiO.

The specific surface area of the NiO nanoparticles obtained from the decomposition of complex at 400 °C for 1 h was measured to be 84.5 m^2/g by the BET method. The particle size was also calculated from the data of specific surface area by the equation: $D_{BET} = 6000/(\rho \times S_{BET})$, where D_{BET} is the diameter of a spherical particle, ρ is the theoretical density of NiO in g/cm^3 and S_{BET} is the specific surface area of NiO powder in m^2/g. The particle size calculated from the surface area, assuming spherical particles, is about 17 nm, which is in good agreement with the XRD and TEM results described above.

Fig. 6 represents the UV–Vis spectrum of the NiO nanoparticles, with a strong absorption band in the UV–Vis region (λ_{max} = 325 nm), indicating that the NiO nanoparticles prepared by this method could be a promising photocatalytic material. This absorption band is attributed to the electronic transition from the valence band to the conduction band in the NiO semiconductor. The direct optical band gap (E_g) of the NiO nanoparticles can be estimated by

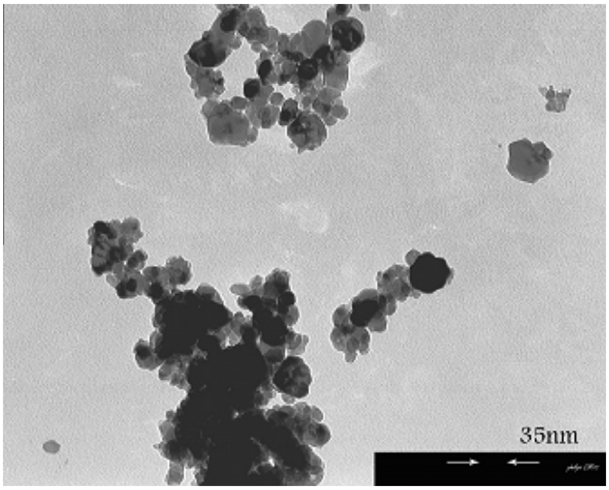

Fig. 5. TEM image of the NiO nanoparticles.

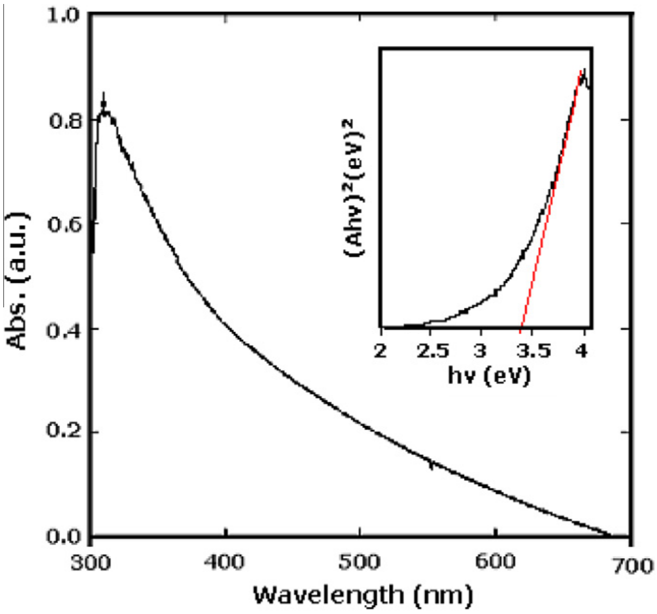

Fig. 6. UV–Vis spectrum of the NiO nanoparticles.

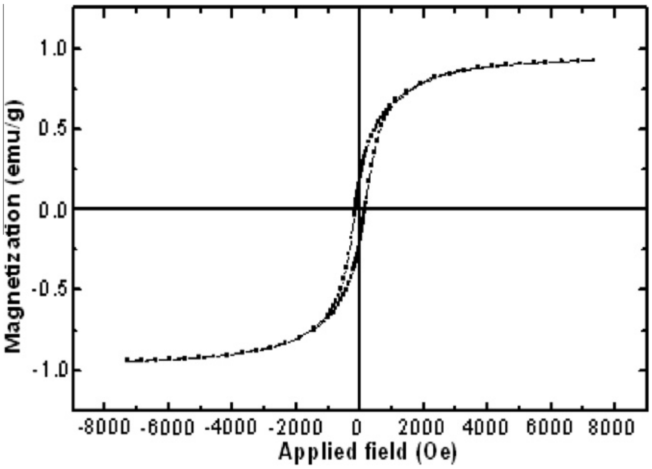

Fig. 7. Magnetization versus applied magnetic field at room temperature for the NiO nanoparticles prepared at 400 °C.

the equation: $(Ah\nu)^2 = B(h\nu - E_g)$, where $h\nu$ is the photon energy, A is the absorption coefficient, B is a constant relative to the material. The inset of Fig. 6 shows the $(Ah\nu)^2 \sim h\nu$ curve for the NiO sample calcined at 400 °C. By extrapolation of this curve, the band gap is 3.4 eV, revealing a slight red shift in comparison with previous reports [45–47].

Fig. 7 shows the magnetization versus applied magnetic field curve at room temperature for the NiO nanoparticles prepared at 400 °C. The hysteresis loop shows a ferromagnetic behavior for the NiO nanoparticles with a remnant magnetization (M_r) of 0.25 emu/g, which is quite different from the bulk sample [32,48]. The coercive field (H_c) and the saturation magnetization (M_s) are about 160 Oe and 0.9 emu/g, respectively. The origin of the ferromagnetic property may be attributed to the size confinement effect of the NiO nanoparticles [49,50]. Nickel oxide nanoparticles are made of small magnetic domains. Each magnetic domain is characterized by its own magnetic moment oriented randomly. The total magnetic moment of the nanoparticles is the sum of these magnetic domains coupled by dipolar interactions. As a result, a low value of M_s is obtained. The magnetic properties of nanomaterials have been believed to be highly dependent on the sample shape, crystallinity, magnetization direction and so on.

4. Conclusions

In summary, pure and nanosized NiO particles with an average particle size of 15 nm were successfully synthesized through thermal decomposition of the $[Ni(en)_3](NO_3)_2$ complex as a precursor at 400 °C. From this complex, NiO is formed via the explosive decomposition of the $[Ni(en)_3](NO_3)_2$ complex due to a redox process taking place between the reductants (en ligands) and the oxidants (NO_3^-). By this method, uniform and spherical NiO nanoparticles with weak agglomeration, narrow size distribution and ferromagnetic behavior can be obtained. The optical absorption band gap of the NiO nanoparticles is 3.4 eV, which shows a red shift in comparison with the bulk sample. This method is simple, low-cost, safe and suitable for industrial production of high purity NiO nanoparticles for various applications. We expect that this method of precursor thermal decomposition can be extended to synthesize nanoparticles of other kinds of metal oxides using the corresponding precursors.

Acknowledgments

The authors gratefully acknowledge the Lorestan University Research Council and Iran Nanotechnology Initiative Council (INIC) for their financial support.

References

[1] G. Schmidt, Nanoparticles: From Theory to Application, VCH, Weinheim, 2004.
[2] E.T. Goldvurt, B. Kulkarni, R.N. Bhargava, J. Lumin. 72 (1997) 190.
[3] E.F. Hilinske, P.A. Lucas, Y. Wang, J. Chem. Phys. 89 (1988) 3435.
[4] N.R. Jana, Y.F. Chen, X.G. Peng, Chem. Mater. 16 (2004) 3931.
[5] A. Chrissanthopoulos, S. Baskoutas, N. Bouropoulos, V. Dracopoulos, P. Poulopoulos, S.N. Yannopoulos, Photonics and Nanostructures – Fundamentals and Applications, doi:10.1016/j.photonics.2010.11.002.
[6] W. Wei, X. Jiang, L. Lu, X. Yang, X. Wang, J. Hazard. Mater. 168 (2009) 838.
[7] Nagi R.E. Radwan, M.S. El-Shall, Hassan M.A. Hassan, Appl. Catal. A: Gen. 331 (2007) 8.
[8] J.L. Garcia-Miquel, Q. Zhang, S.J. Allen, A. Rougier, A. Blyr, H.O. Davies, Thin Solid Films 424 (2003) 165.
[9] W.Y. Li, L.N. Xu, J. Chen, Adv. Funct. Mater. 15 (2005) 851.
[10] F. Li, H.Y. Chen, C.M. Wang, K.S. Hu, J. Electroanal. Chem. 531 (2002) 53.
[11] I. Hotovy, J. Huran, L. Spiess, S. Hascik, V. Rehacek, Sens. Actuators B: Chem. 57 (1999) 147.
[12] H.X. Yang, Q.F. Dong, X.H. Hu, J. Power Sources 79 (1999) 256.
[13] F.B. Zhang, Y.K. Zhou, H.L. Li, Mater. Chem. Phys. 83 (2004) 260.
[14] X.H. Huang, J.P. Tu, B. Zhang, C.Q. Zhang, Y. Li, Y.F. Yuan, H.M. Wu, J. Power Sources 161 (2006) 541.
[15] M. Ghosh, K. Biswas, A. Sundaresan, C.N.R. Rao, J. Mater. Chem. 16 (2006) 106.
[16] T. Ahmad, K.V. Ramanujachary, S.E. Lofland, A.K. Ganguli, Solid State Sci. 8 (2006) 425.
[17] M. Borgstrom, E. Blart, G. Boschloo, E. Mukhtar, A. Hagfeldt, L. Hammarstrom, J. Phys. Chem. B 109 (2005) 22928.
[18] T. Nathan, A. Aziz, A.F. Noor, S.R.S. Prabaharan, J. Solid State Electrochem. 12 (2008) 1003.
[19] C.G. Granqvist (Ed.), Handbook of Inorganic Electrochromic Materials, Elsevier, Amsterdam, 1995.
[20] X.Y. Deng, Z. Chen, Mater. Lett. 58 (2004) 276.
[21] V.R.R. Pulimi, P. Jeevanandam, J. Magn. Magn. Mater. 321 (2009) 2556.
[22] S.F. Wang, L.Y. Shi, X. Feng, Sh.R. Ma, Mater. Lett. 61 (2007) 1549.
[23] D.Y. Han, H.Y. Yang, C.B. Shen, X. Zhou, F.H. Wang, Powder Tech. 147 (2004) 113.
[24] P. Palanisamy, A.M. Raichur, Mater. Sci. Eng. C 29 (2009) 199.
[25] D.V. Lysov, D.V. Kuznetsov, A.G. Yudin, D.S. Muratov, V.V. Levina, D.I. Ryzhonkov, Nanotechnologies in Russia 5 (2010) 493.
[26] E.R. Beach, K. Shqau, S.E. Brown, S.J. Rozeveld, P.A. Morris, Mater. Chem. Phys. 115 (2009) 371.
[27] E. Beach, S. Brown, K. Shqau, M. Mottern, Z. Warchol, P. Morris, Mater. Lett. 62 (2008) 1957.
[28] Z. Wei, H. Qiao, H. Yang, C. Zhang, X. Yan, J. Alloys Compd. 479 (2009) 855.
[29] T.L. Lai, Y.Y. Shub, G.L. Huangb, C.C. Lee, C.B. Wang, J. Alloys Compd. 450 (2008) 318.
[30] A. Surca, B. Orel, B. Pihlar, P. Bukovec, J. Electroanal. Chem. 408 (1996) 83.
[31] Y. Wu, Y. He, T. Wu, T. Chen, W. Weng, H. Wan, Mater. Lett. 61 (2007) 3174.
[32] S. Thota, J. Kumar, J. Phys. Chem. Solids 68 (2007) 1951.
[33] W.N. Wang, Y. Itoh, I.W. Lenggoro, K. Okuyama, Mater. Sci. Eng. B 111 (2004) 69.
[34] I.W. Lenggoroa, Y. Itoh, N. Iid, K. Okuyama, Mater. Res. Bull. 38 (2003) 1819.
[35] E. Traversa, M. Sakamoto, Y. Sadaoka, Part. Sci. Technol. 16 (1998) 185.
[36] M. Salavati-Niasari, F. Mohandes, F. Davar, M. Mazaheri, M. Monemzadeh, N. Yavarinia, Inorg. Chim. Acta 362 (2009) 3691.
[37] F. Davar, Z. Fereshteh, M. Salavati-Niasari, J. Alloys Compd. 476 (2009) 797.
[38] M. Salavati-Niasari, N. Mir, F. Davar, Polyhedron 28 (2009) 1111.
[39] X. Li, X. Zhang, Z. Li, Y. Qian, Solid State Commun. 137 (2006) 581.
[40] S. Farhadi, N. Rashidi, J. Alloys Compd. 503 (2010) 439.
[41] S. Farhadi, N. Rashidi, Polyhedron 503 (2010) 439.
[42] H.P. Klug, L.E. Alexander, X-ray Diffraction Procedures, second ed., Wiley, New York, 1964.
[43] K. Nakamoto, Infrared and Raman Spectra of Inorganic and Coordination Compounds Part B: Applications in Coordination, sixth ed., Organometallic and Bioinorganic Chemistry, Wiley, New York, 2009.
[44] C. Wang, C. Shao, L. Wang, L. Zhang, X. Li, Y. Liu, J. Colloid Interface Sci. 333 (2009) 242.
[45] G. Boschloo, A. Hagfeldt, J. Phys. Chem. B. 195 (2001) 3039.
[46] X. Chen, Z. Zhang, C. Shi, X. Li, Mater. Lett. 62 (2008) 346.
[47] Z. Chen, A. Xu, Y. Zhang, N. Gu, Curr. Appl. Phys. 10 (2010) 967.
[48] A.T. Ngo, P. Bonville, M.P. Pileni, Eur. Phys. J. B 9 (1999) 583.
[49] M. Salavati-Niasari, Z. Fereshteh, F. Davar, Polyhedron 28 (2009) 1065.
[50] Q. Li, L.S. Wang, B.Y. Hu, C. Yang, L. Zhou, L. Zhang, Mater. Lett. 61 (2007) 1615.